LETTER

https://doi.org/10.1038/s41586-018-0324-7

53BP1–RIF1–shieldin counteracts DSB resection through CST- and Polα-dependent fill-in

Zachary Mirman[1,5], Francisca Lottersberger[1,4,5], Hiroyuki Takai[1], Tatsuya Kibe[1], Yi Gong[1], Kaori Takai[1], Alessandro Bianchi[1,2], Michal Zimmermann[1,3], Daniel Durocher[3] & Titia de Lange[1]*

In DNA repair, the resection of double-strand breaks dictates the choice between homology-directed repair—which requires a 3′ overhang—and classical non-homologous end joining, which can join unresected ends[1,2]. BRCA1-mutant cancers show minimal resection of double-strand breaks, which renders them deficient in homology-directed repair and sensitive to inhibitors of poly(ADP-ribose) polymerase 1 (PARP1)[3–8]. When BRCA1 is absent, the resection of double-strand breaks is thought to be prevented by 53BP1, RIF1 and the REV7–SHLD1–SHLD2–SHLD3 (shieldin) complex, and loss of these factors diminishes sensitivity to PARP1 inhibitors[4,6–9]. Here we address the mechanism by which 53BP1–RIF1–shieldin regulates the generation of recombinogenic 3′ overhangs. We report that CTC1–STN1–TEN1 (CST)[10], a complex similar to replication protein A that functions as an accessory factor of polymerase-α (Polα)–primase[11], is a downstream effector in the 53BP1 pathway. CST interacts with shieldin and localizes with Polα to sites of DNA damage in a 53BP1- and shieldin-dependent manner. As with loss of 53BP1, RIF1 or shieldin, the depletion of CST leads to increased resection. In BRCA1-deficient cells, CST blocks RAD51 loading and promotes the efficacy of PARP1 inhibitors. In addition, Polα inhibition diminishes the effect of PARP1 inhibitors. These data suggest that CST–Polα-mediated fill-in helps to control the repair of double-strand breaks by 53BP1, RIF1 and shieldin.

This study was initiated to determine whether the control of 5′ resection at double-strand breaks (DSBs) resembles the regulation of resection at telomeres. The formation of telomeric t-loops requires the generation of 3′ overhangs after DNA replication[12–15]. Newly replicated telomeres are resected by EXO1, which generates 3′ overhangs that are too long and require fill-in mediated by Polα–primase[16] (Fig. 1a). Polα–primase is brought to telomeres by an interaction between CST (also known as α-accessory factor, AAF[11,17]) and POT1B in mouse shelterin[16] (Fig. 1a). Here we test whether CST–Polα fill-in of 3′ overhangs has a role in the regulation of DSB resection by 53BP1, RIF1 and shieldin.

To study the role of CST at sites of DNA damage we used telomeres that lack shelterin protection, which are a model system for DSB resection[8,15,18–20]. Hyper-resection occurs upon Cre-mediated removal of TPP1 (and POT1A and POT1B) from telomeres of *Tpp1*$^{f/f}$ mouse embryo fibroblasts (MEFs). This hyper-resection is counteracted by 53BP1 and RIF1[20], which accumulate in response to ATR signalling at telomeres that lack POT1A (Fig. 1a). As does 53BP1, shieldin limited hyper-resection at telomeres that lack TPP1: TPP1-deficient cells that lacked either REV7 or SHLD2 showed telomere hyper-resection (Fig. 1b–d, Extended Data Fig. 1a–c).

As CST is essential[21,22], we used short hairpin RNAs (shRNAs) to explore the role of CST in telomere hyper-resection. Depletion of STN1 or CTC1 increased the telomeric overhang signal in cells that lack TPP1 (Fig. 1b–d, Extended Data Figs. 1d, 2), and tests with *Escherichia coli* ExoI confirmed that the signal derived from a 3′ overhang (Extended Data Fig. 1e, f). Knockdown of STN1 or CTC1 did not affect the resection at telomeres when TPP1 was deleted from REV7-deficient cells (Fig. 1b–d, Extended Data Fig. 2). Furthermore, STN1 knockdown had no effect on telomere hyper-resection when either 53BP1 or RIF1 were absent, or when cells contained a form of 53BP1 that does not recruit RIF1[23] (Extended Data Fig. 3). These data suggest that CST acts in a 53BP1-, RIF1- and shieldin-dependent manner to limit the formation of single-stranded DNA at dysfunctional telomeres.

To determine whether CST also counteracted resection at sites of ATM signalling, we used conditional deletion of *Trf2* (Fig. 1e). Telomeres that lack TRF2 undergo fusion mediated by classical non-homologous end joining[24–26]. In cells deficient in DNA ligase IV (LIG4), in which such telomere fusions are prevented[26], telomeres that lack TRF2 undergo 5′-end resection that is exacerbated by loss of 53BP1 or RIF1[8,19] (Fig. 1e). Similarly, the 5′-end resection was increased by REV7 or SHLD2 deficiency (Fig. 1f–h, Extended Data Fig. 4). When STN1 was depleted from cells that lack TRF2, resection at telomeres was significantly increased (Fig. 1f–h) and this effect was epistatic with REV7 (Fig. 1f–h). Thus, CST counteracts resection in a shieldin-dependent manner in the context of ATM signalling.

We next determined whether CST localized to damaged telomeres in a 53BP1- and shieldin-dependent manner. Myc-tagged CTC1 was detectable at telomeres with functional shelterin, whereas in cells that are deficient in POT1B—which show extended telomeric 3′ overhangs but no DNA damage signalling[27]—the localization of CTC1 at telomeres was minimal (Fig. 2a, b). When ATR was activated by deletion of *Tpp1* (Fig. 2a, right), CTC1 was again detectable at telomeres (Fig. 2a, b) despite the absence of POT1B. The recruitment of CTC1 to dysfunctional telomeres depended on ATR signalling, 53BP1 and shieldin (Fig. 2b, c). Similarly, Cre-mediated deletion of the single human POT1 protein from conditional *POT1*-knockout HT1080 cells[28] led to telomeric accumulation of STN1 that required ATR kinase (Fig. 2d–f). Thus, CST localizes to damaged telomeres in a shieldin-dependent manner.

Co-immunoprecipitation experiments showed that shieldin components could associate with CST (Fig. 2g, Extended Data Fig. 5a). In a yeast two-hybrid assay, CTC1 robustly interacted with SHLD1 and STN1 interacted with SHLD3 (Fig. 2h, Extended Data Fig. 5b). Weaker interactions were detectable between TEN1 and SHLD3; STN1 and SHLD1, SHLD2 or REV7; and CTC1 and REV7. Thus, shieldin binds CST through multiple direct interactions.

In human cells, STN1 co-localized with 53BP1 at DSBs induced by ionizing radiation (Fig. 3a, b) in a manner dependent on shieldin (Fig. 3b). Furthermore, STN1 was detectable at DSBs induced by FOKI in U2OS cells. This localization was diminished upon inhibition of ATM and ATR signalling, and required 53BP1 and shieldin (Fig. 3c–e, Extended Data Fig. 6a), which indicates that CST is recruited to sites of DNA damage by shieldin.

Because CST is associated with Polα–primase, we examined the localization of Polα at DSBs. Because Polα forms numerous S-phase foci (Extended Data Fig. 6b), we examined cells arrested in G2 (Fig. 3f,

[1]Laboratory for Cell Biology and Genetics, Rockefeller University, New York, NY, USA. [2]Genome Damage and Stability Centre, School of Life Sciences, University of Sussex, Brighton, UK. [3]Lunenfeld-Tanenbaum Research Institute, Mount Sinai Hospital, Toronto, Canada. [4]Present address: Department of Medical and Health Sciences, Linköping University, Linköping, Sweden. [5]These authors contributed equally: Zachary Mirman, Francisca Lottersberger. *e-mail: delange@rockefeller.edu

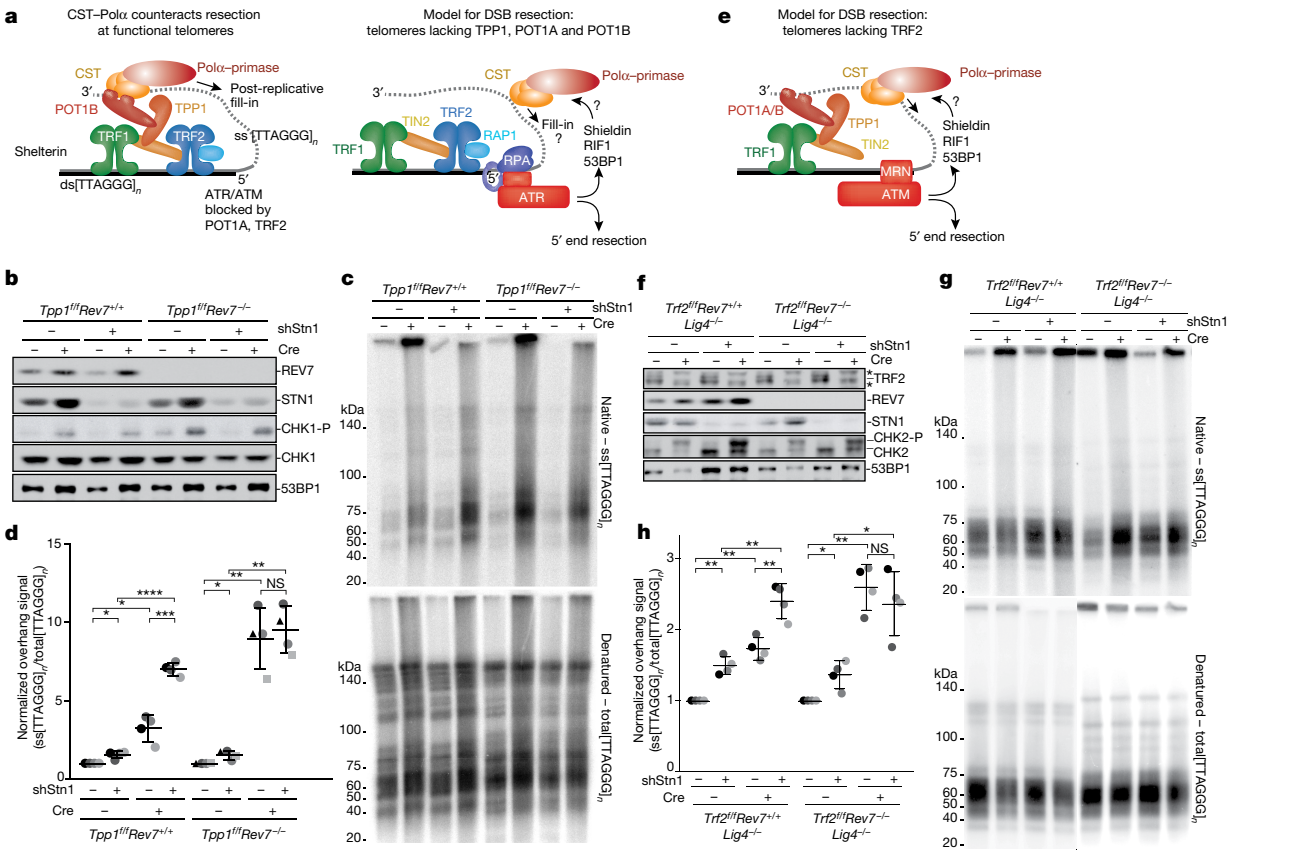

Fig. 1 | Shieldin and CST counteract resection at dysfunctional telomeres. a, Left, schematic showing POT1B-bound CST counteracting the resection of telomere ends. Right, depiction of telomeres that lack TPP1, POT1A and POT1B as a proxy for DSB resection. Telomeres that lack TPP1 undergo ATR-dependent hyper-resection that is repressed by 53BP1. **b**, Immunoblots showing loss of REV7 and STN1 in the indicated $Tpp1^{f/f}Rev7^{+/+}$ (*Rev7* is also known as *Mad2l2*) MEFs and $Tpp1^{f/f}Rev7^{-/-}$ (CRISPR) clones treated with Cre (96 h) and/or *Stn1* shRNA (shStn1) as indicated. CHK1-P serves as a proxy for TPP1 deletion. **c**, Quantitative analysis of telomere end resection in the cells shown in **b** using in-gel hybridization to detect the 3′ overhang (top), followed by rehybridization to the denatured DNA in the same gel (bottom) to determine the ratio of single-stranded (ss) TTAGGG to total TTAGGG signal. Representative of four experiments. **d**, Quantification of resection detected in **c**, determined from four independent experiments (different shades of grey) and showing mean and s.d. Three independent *Rev7* knockout clones were used (distinct symbols). **e**, Telomeres that lack TRF2 as a model for resection upon ATM activation. **f**, Immunoblots showing Cre-mediated deletion of TRF2 from $Trf2^{f/f}Lig4^{-/-}$ (*Trf2* is also known as *Terf2*) cells, CRISPR deletion of *Rev7*, shRNA-mediated reduction of STN1 and CHK2 phosphorylation. Asterisk, non-specific band. **g**, **h**, Telomere end resection analysis on the cells in **f**, as in **c**, **d**. Mean and s.d. from four independent experiments using two clones of each genotype. Note that the order of the samples is different in **h** when compared to **f**, **g**. All data panels in the figure are representative of four experiments. Mean indicated with centre bars and s.d. with error bars. $*P<0.05$, $**P<0.01$, $***P<0.001$, $****P<0.0001$, NS, not significant, two-tailed Welch's *t*-test.

Extended Data Fig. 6c). In cells that expressed HA-tagged STN1, Polα co-localized with STN1 at DSBs induced by FOKI (Fig. 3f, Extended Data Fig. 6c). The localization of Polα to DSBs was diminished upon inhibition of ATM and ATR signalling, and required 53BP1 and shieldin (Fig. 3f, Extended Data Fig. 6d), which demonstrates that Polα and CST require the same factors for their localization to DSBs.

Depletion of STN1 increased the percentage of cells that contained replication protein A (RPA) foci after exposure to ionizing radiation (Fig. 3g, i), increased the signal intensity of the RPA foci (Fig. 3h) and increased the overall RPA signal intensity per nucleus (Extended Data Fig. 7). Furthermore, deletion of CTC1 from a human HCT116 cell line[21] led to an increase in the phosphorylation of RPA upon irradiation (Fig. 3j) and CST depletion increased phosphorylation of RPA in irradiated MEFs (Fig. 3k). In cells that lack BRCA1, depletion of CST also increased the percentage of cells with RAD51 foci induced by ionizing radiation (Fig. 3l, m), which suggests that this depletion restores homology-directed repair. Conversely, on the basis of an assay for the fusion of telomeres that lack TRF2[26], it appears that the depletion of CST diminishes classical non-homologous end joining (Fig. 3n, o).

BRCA1-deficient cells become resistant to treatment with PARP1 inhibitors (PARPi) when 53BP1, RIF1 or shieldin are absent[3–9]. Similarly, STN1 or CTC1 depletion from $Brca1^{f/f}$ MEFs reduced the lethality of PARPi in BRCA1-deficient cells (Fig. 4a, b, Extended Data Fig. 8a–f). By contrast, in $Brca1^{f/f}$ subclones that lack 53BP1 or REV7, depletion of CTC1 or STN1 did not affect resistance to PARPi (Fig. 4c, Extended Data Fig. 8c–f). Furthermore, in BRCA1-deficient cells, CST depletion reduced the radial chromosomes induced by PARPi (Fig. 4d, e) and this effect was epistatic with 53BP1 and REV7 (Fig. 4e). These data are consistent with CST acting together with 53BP1 and shieldin to minimize formation of single-stranded DNA at DSBs.

To examine the consequences of Polα inhibition in PARPi-treated BRCA1-deficient cells without confounding S-phase effects, cells were arrested in G2 before addition of Polα inhibitors (Fig. 4f). Cells that experienced Polα inhibition in G2 showed reduced formation of radial chromosomes (Fig. 4f, Extended Data Fig. 8g). BrdU incorporation experiments confirmed that the mitotic cells we collected had passed through S phase during treatment with PARPi (Extended Data Fig. 8h–j). The effect of Polα inhibition with 10 μm CD437 was not exacerbated by depletion of CST (Fig. 4f). Collectively, these data are consistent with CST and Polα acting to limit the formation of recombinogenic 3′ overhangs at DSBs in BRCA1-deficient cells (Fig. 4g).

Our data suggest a sophisticated mechanism by which 53BP1 and shieldin act together with CST and Polα to fill in resected DSBs. At

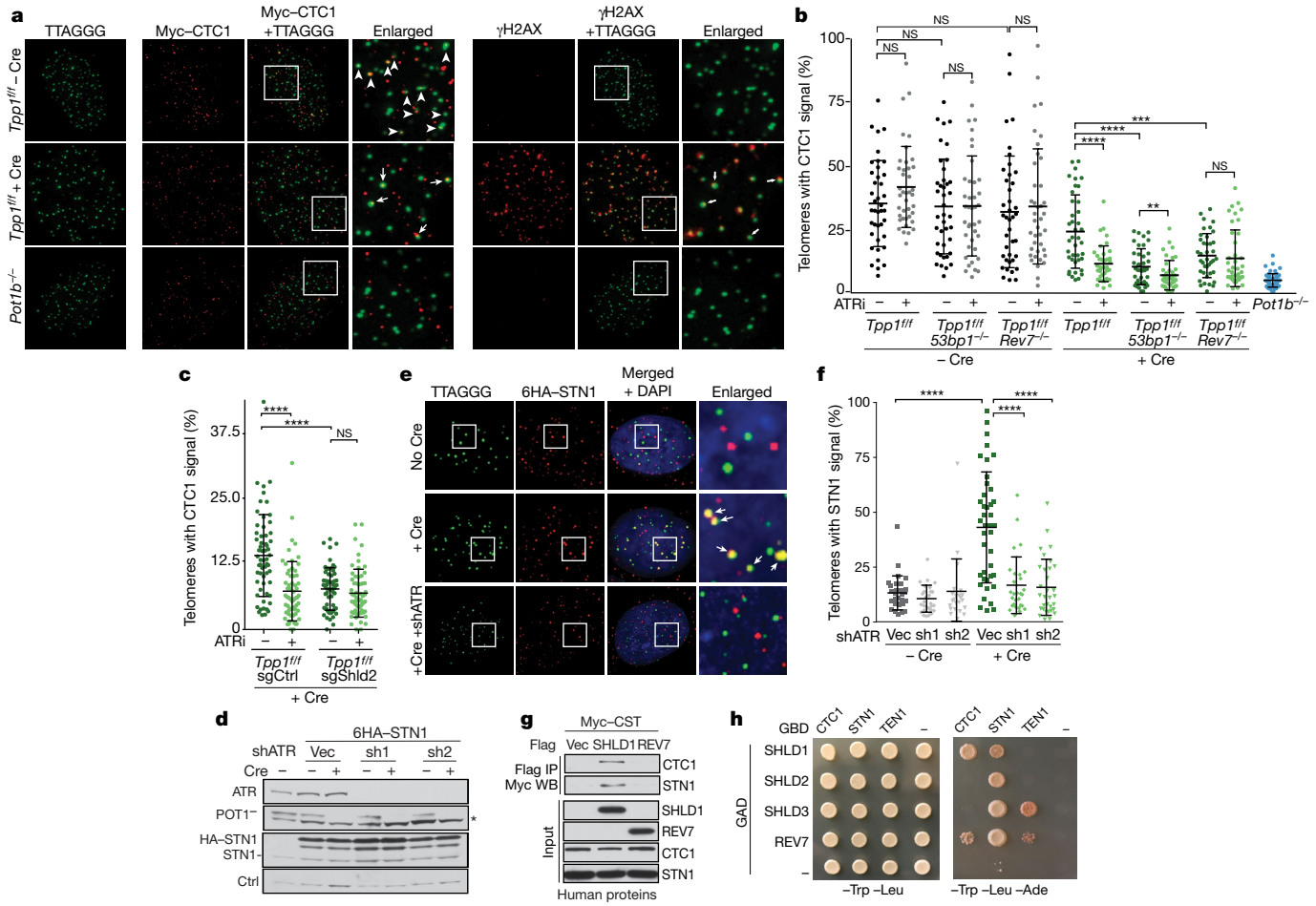

Fig. 2 | 53BP1- and shieldin-dependent localization of CST to dysfunctional telomeres. a, Left, representative immunofluorescence and fluorescence in situ hybridization (IF–FISH) for 6×-Myc-tagged CTC1 (red) at telomeres (false-coloured in green) in *Tpp1*$^{f/f}$ MEFs before and after Cre (96 h). Arrowheads, CTC1 at telomeres. *Pot1b*$^{-/-}$ cells control for spurious telomere–CTC1 co-localization. Right, the same nuclei showing γH2AX (red) at telomeres that lack TPP1. The γH2AX and CTC1 signals are both false-coloured in red. Arrows, telomeres with CTC1 and γH2AX. **b**, Quantification of the percentage of telomeres co-localizing with CTC1, detected as in **a**. Each dot represents one nucleus from the indicated *Tpp1*$^{f/f}$ cell lines with and without Cre and/or ATR inhibitor (ATRi). *53bp1* is also known as *Trp53bp1*. Mean and s.d. from three independent experiments. **c**, As in **b**, but using *Tpp1*$^{f/f}$ cells treated with a *Shld2* single-guide RNA (sgRNA) (sgShld2) or a control sgRNA (sgCtrl). Mean and s.d. as in **b**. **d**, Immunoblots for POT1 deletion, ATR knockdown and HA-tagged STN1 (6HA–STN1) in conditional *POT1*-knockout human HT1080 cells. Asterisk, non-specific band. sh1 and sh2 denote two different *ATR* shRNAs (see Methods for details). **e**, IF–FISH showing telomeric DNA co-localizing with STN1 in cells as in **d**, treated with Cre (96 h) and *ATR* shRNAs. **f**, Quantification of STN1 localization at telomeres before and after *POT1* deletion, with or without *ATR* shRNAs as in **e**. Mean and s.d. from three independent experiments. Each symbol represents one nucleus. **g**, Immunoprecipitation of human CST (each subunit Myc-tagged) with Flag-tagged human SHLD1 or REV7 co-expressed in 293T cells. **h**, Yeast two-hybrid assay for interaction between CST and shieldin subunits. All data panels in the figure are representative of three experiments. Mean indicated with centre bars and s.d. with error bars. GAD, Gal4 activation domain; GBD, Gal4 DNA-binding domain; Vec, empty vector. $^{**}P < 0.01$, $^{***}P < 0.001$, $^{****}P < 0.0001$, two-tailed Welch's *t*-test.

telomeres, the POT1–TPP1 heterodimer recruits CST–Polα–primase to fill in part of the 3′ overhang formed after telomere end resection (Fig. 4g). We propose that at sites of DNA damage, shieldin recruits CST–Polα–primase for the purpose of filling in resected DSBs. In both settings, CST is tethered, allowing CST to engage single-stranded DNA despite its modest affinity for this substrate[29] and enabling regulation of the fill-in reaction through recruitment. Recent data have shown that 53BP1 represses mutagenic single-strand annealing, possibly by preventing excessive resection[30]. Our findings regarding CST–Polα could explain this observation. At telomeres, partial fill-in by CST–Polα counteracts hyper-resection but leaves a 3′ overhang that can form a t-loop, a process similar to the initiation of homology-directed repair[12,13]. At DSBs, CST–Polα could similarly counteract hyper-resection—and thus single-strand annealing—and generate a 3′ overhang that is sufficient for homology-directed repair. In BRCA1-deficient cells, this fill-in reaction, together with the persistence of CST–shieldin at the DSBs, could block homology-directed repair and result in lethal mis-repair.

Online content

Any Methods, including any statements of data availability and Nature Research reporting summaries, along with any additional references and Source Data files, are available in the online version of the paper at https://doi.org/10.1038/s41586-018-0324-7.

Received: 2 January 2018; Accepted: 10 May 2018;
Published online 18 July 2018.

1. Zimmermann, M. & de Lange, T. 53BP1: pro choice in DNA repair. *Trends Cell Biol.* **24**, 108–117 (2014).
2. Panier, S. & Boulton, S. J. Double-strand break repair: 53BP1 comes into focus. *Nat. Rev. Mol. Cell Biol.* **15**, 7–18 (2014).
3. Bouwman, P. et al. 53BP1 loss rescues BRCA1 deficiency and is associated with triple-negative and BRCA-mutated breast cancers. *Nat. Struct. Mol. Biol.* **17**, 688–695 (2010).
4. Xu, G. et al. REV7 counteracts DNA double-strand break resection and affects PARP inhibition. *Nature* **521**, 541–544 (2015).
5. Bunting, S. F. et al. 53BP1 inhibits homologous recombination in *Brca1*-deficient cells by blocking resection of DNA breaks. *Cell* **141**, 243–254 (2010).

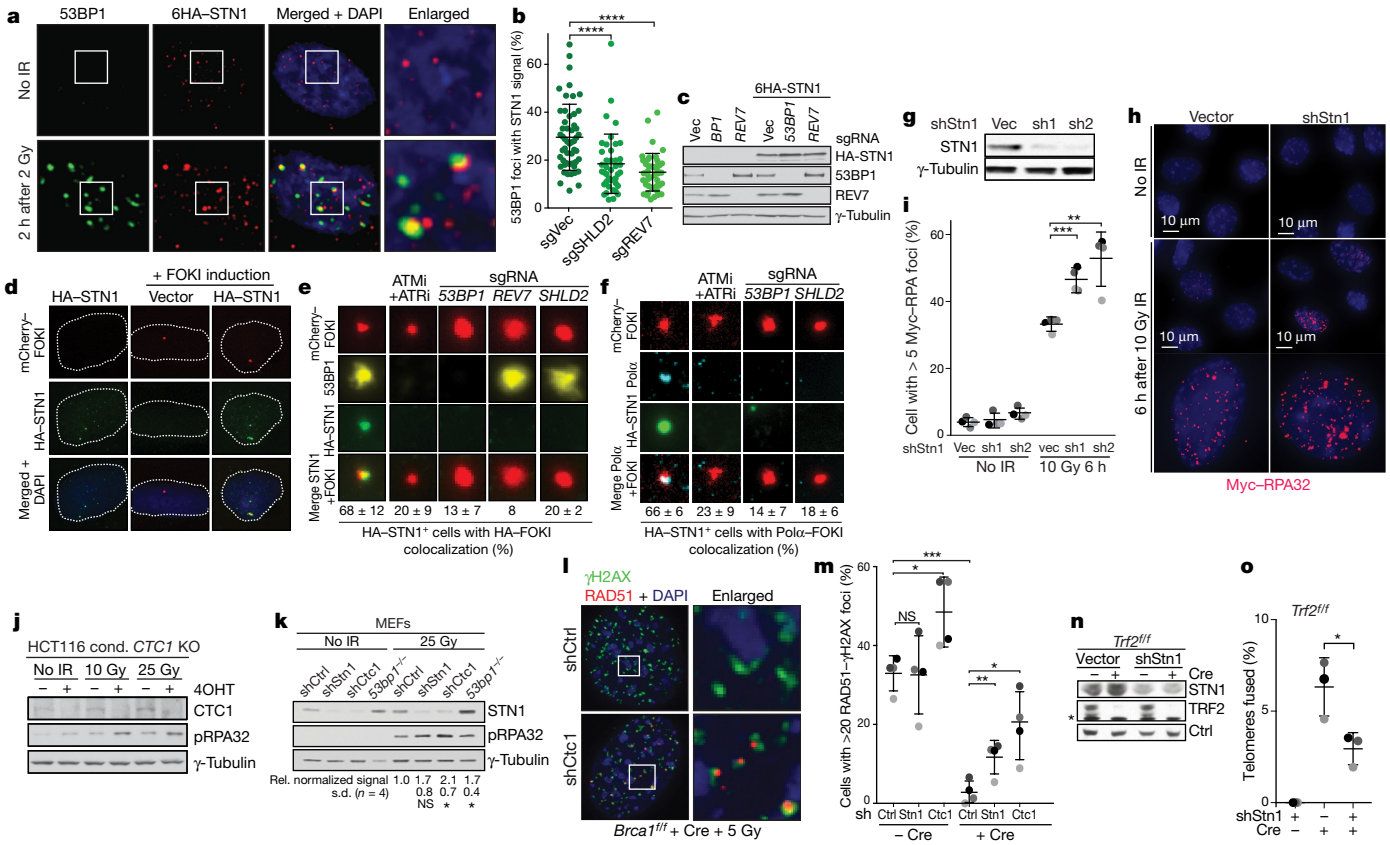

Fig. 3 | CST localizes to DSBs and represses formation of single-stranded DNA. a, Immunofluorescence for 53BP1 and HA–STN1 in HT1080 cells treated with ionizing radiation. **b**, Quantification of 53BP1–STN1 co-localization as in **a**, in cells with the indicated sgRNAs. Mean and s.d. from three independent experiments, >15 nuclei per experiment for each experimental setting. **c**, Immunoblots for the indicated proteins in FOKI–LacI U2OS cells treated with the indicated sgRNAs. *53BP1* is also known as *TRP53BP1*. **d**, Immunofluorescence for mCherry–FOKI (red) and HA–STN1 (green) in FOKI–LacI U2OS cells as in **c**. **e**, Examples of HA–STN1 co-localizing with FOKI foci in cells as in **d**, treated with ATM inhibitor (ATMi) and ATRi, or the indicated sgRNAs and quantification of STN1–FOKI co-localization. Mean and s.d. from three independent experiments with >80 induced nuclei analysed for each condition. **f**, As in **e**, but monitoring Polα at DSBs in G2-arrested cells that express HA–STN1. **g**, Immunoblot for STN1 knockdown in MEFs that express Myc–RPA32. sh1 and sh2 denote two different *Stn1* shRNAs (see Methods for details). **h**, Immunofluorescence for Myc–RPA32 after 10 Gy ionizing radiation (6 h) in MEFs. **i**, Quantification of cells with RPA foci as in **h**, in >30 nuclei for each condition in four independent experiments (grey shading) with mean and s.d. **j**, **k**, Immunoblots for ionizing radiation-induced RPA phosphorylation (pRPA32, phosphorylated at Ser4 and Ser8) after deletion of *CTC1* from human cells (**j**) or after depletion of STN1, CTC1 or 53BP1 from MEFs (**k**). **l**, Immunofluorescence for RAD51–γH2AX co-localization at DSBs induced by ionizing radiation, in BRCA1-deficient cells treated with *Ctc1* shRNA. **m**, Quantification of data in **l**. Mean and s.d. from four independent experiments (grey shading), >60 nuclei per experiment. **n**, Immunoblot for STN1 knockdown and TRF2 deletion from $Trf2^{f/f}Rosa^{creER}$ MEFs. Asterisk denotes non-specific band. **o**, Effect of STN1 knockdown on telomere–telomere fusions. Mean and s.d. from three independent experiments with >6,000 telomeres each. All immunofluorescence and immunoblots shown are representative of three experiments. Mean indicated with centre bars and s.d. with error bars. IR, ionizing radiation; KO, knockout. $^{*}P < 0.05$, $^{**}P < 0.01$, $^{***}P < 0.001$, $^{****}P < 0.0001$, two-tailed Welch's *t*-test.

6. Chapman, J. R. et al. RIF1 is essential for 53BP1-dependent nonhomologous end joining and suppression of DNA double-strand break resection. *Mol. Cell* **49**, 858–871 (2013).
7. Boersma, V. et al. MAD2L2 controls DNA repair at telomeres and DNA breaks by inhibiting 5′ end resection. *Nature* **521**, 537–540 (2015).
8. Zimmermann, M., Lottersberger, F., Buonomo, S. B., Sfeir, A. & de Lange, T. 53BP1 regulates DSB repair using Rif1 to control 5′ end resection. *Science* **339**, 700–704 (2013).
9. Noordermeer, S. M. et al. The shieldin complex mediates 53BP1-dependent DNA repair. *Nature* https://doi.org/10.1038/s41586-018-0340-7 (2018).
10. Price, C. M. et al. Evolution of CST function in telomere maintenance. *Cell Cycle* **9**, 3177–3185 (2010).
11. Casteel, D. E. et al. A DNA polymerase-α·primase cofactor with homology to replication protein A-32 regulates DNA replication in mammalian cells. *J. Biol. Chem.* **284**, 5807–5818 (2009).
12. Griffith, J. D. et al. Mammalian telomeres end in a large duplex loop. *Cell* **97**, 503–514 (1999).
13. Doksani, Y., Wu, J. Y., de Lange, T. & Zhuang, X. Super-resolution fluorescence imaging of telomeres reveals TRF2-dependent T-loop formation. *Cell* **155**, 345–356 (2013).
14. Palm, W. & de Lange, T. How shelterin protects mammalian telomeres. *Annu. Rev. Genet.* **42**, 301–334 (2008).
15. Lazzerini-Denchi, E. & Sfeir, A. Stop pulling my strings–what telomeres taught us about the DNA damage response. *Nat. Rev. Mol. Cell Biol.* **17**, 364–378 (2016).
16. Wu, P., Takai, H. & de Lange, T. Telomeric 3′ overhangs derive from resection by Exo1 and Apollo and fill-in by POT1b-associated CST. *Cell* **150**, 39–52 (2012).
17. Goulian, M., Heard, C. J. & Grimm, S. L. Purification and properties of an accessory protein for DNA polymerase α/primase. *J. Biol. Chem.* **265**, 13221–13230 (1990).
18. Sfeir, A. & de Lange, T. Removal of shelterin reveals the telomere end-protection problem. *Science* **336**, 593–597 (2012).
19. Lottersberger, F., Bothmer, A., Robbiani, D. F., Nussenzweig, M. C. & de Lange, T. Role of 53BP1 oligomerization in regulating double-strand break repair. *Proc. Natl Acad. Sci. USA* **110**, 2146–2151 (2013).
20. Kibe, T., Zimmermann, M. & de Lange, T. TPP1 blocks an ATR-mediated resection mechanism at telomeres. *Mol. Cell* **61**, 236–246 (2016).
21. Feng, X., Hsu, S. J., Kasbek, C., Chaiken, M. & Price, C. M. CTC1-mediated C-strand fill-in is an essential step in telomere length maintenance. *Nucleic Acids Res.* **45**, 4281–4293 (2017).
22. Gu, P. et al. CTC1 deletion results in defective telomere replication, leading to catastrophic telomere loss and stem cell exhaustion. *EMBO J.* **31**, 2309–2321 (2012).
23. Lottersberger, F., Karssemeijer, R. A., Dimitrova, N. & de Lange, T. 53BP1 and the LINC complex promote microtubule-dependent DSB mobility and DNA repair. *Cell* **163**, 880–893 (2015).
24. van Steensel, B., Smogorzewska, A. & de Lange, T. TRF2 protects human telomeres from end-to-end fusions. *Cell* **92**, 401–413 (1998).
25. Karlseder, J., Broccoli, D., Dai, Y., Hardy, S. & de Lange, T. p53- and ATM-dependent apoptosis induced by telomeres lacking TRF2. *Science* **283**, 1321–1325 (1999).

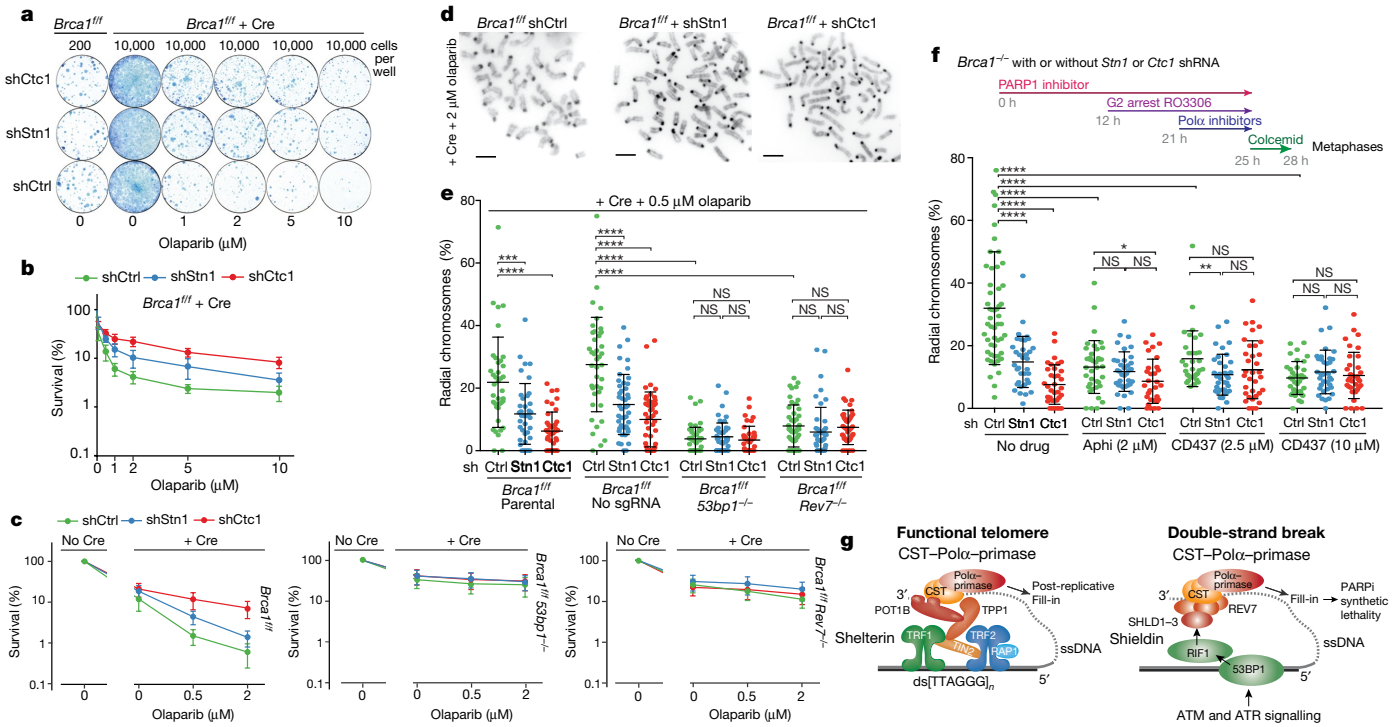

Fig. 4 | CST and Polα affect the outcome of PARPi in BRCA1-deficient cells. a, Colonies detected in a PARPi survival assay using *Brca1*$^{f/f}$ MEFs with or without Cre and *Ctc1* or *Stn1* shRNAs. **b**, Graphical representation of data in **a** from three independent experiments. **c**, Epistasis analysis of PARPi resistance induced by the absence of 53BP1 or REV7, and depletion of CST subunits. Mean (symbol) and s.e.m. (error bars) from three independent experiments. **d**, PARPi-induced radial chromosomes in BRCA1-deficient cells. Scale bars, 1 μm. **e**, Mean (centre bar) and s.d. (error bars) of percentage of misrejoined (radial) chromosomes in >10 metaphases per experimental setting for each of three independent experiments. Each dot represents one metaphase. **f**, Effect of Polα inhibition on radial formation in PARPi-treated *Brca1*$^{-/-}$ cells using the experimental timeline shown. Mean (centre bar) and s.d. (error bars) of the percentage of radial chromosomes in >10 metaphases per experimental setting for each of three independent experiments. Each dot represents one metaphase. Aphi, aphidicolin. **g**, Graphical representation of the similar mechanisms by which resection is counteracted at functional telomeres and at DSBs. **a** and **d** are representative of three experiments. $^{*}P < 0.05$, $^{**}P < 0.01$, $^{***}P < 0.001$, $^{****}P < 0.0001$, two-tailed Welch's *t*-test.

26. Celli, G. B. & de Lange, T. DNA processing is not required for ATM-mediated telomere damage response after TRF2 deletion. *Nat. Cell Biol.* **7**, 712–718 (2005).
27. Hockemeyer, D., Daniels, J. P., Takai, H. & de Lange, T. Recent expansion of the telomeric complex in rodents: two distinct POT1 proteins protect mouse telomeres. *Cell* **126**, 63–77 (2006).
28. Takai, H. et al. A POT1 mutation implicates defective telomere end fill-in and telomere truncations in Coats plus. *Genes Dev.* **30**, 812–826 (2016).
29. Hom, R. A. & Wuttke, D. S. Human CST prefers G-rich but not necessarily telomeric sequences. *Biochemistry* **56**, 4210–4218 (2017).
30. Ochs, F. et al. 53BP1 fosters fidelity of homology-directed DNA repair. *Nat. Struct. Mol. Biol.* **23**, 714–721 (2016).

Acknowledgements We thank D. White for mouse husbandry; N. Bosco, R. Karssemeijer, L. Timashev and Y. Doksani for help with CRISPR gene knockouts, image analysis and generating MEFs; and R. Greenberg and C. Price for providing cell lines. The Rockefeller University BioImaging Center provided assistance. This work was supported by grants from the NCI (R35CA210036), ACS and BCRF to T.d.L., a grant from the CIHR (FDN143343) to D.D. and the Banting Postdoctoral fellowship to M.Z.

Author contributions M.Z. initiated this work in the de Lange laboratory. T.K. and F.L. performed resection assays. Z.M. and H.T. performed CST and Polα localization assays and RPA phosphorylation assays. Z.M. performed PARPi and RAD51 assays. Y.G. and T.K. analysed RPA foci. A.B. performed yeast two-hybrid assays. K.T. and H.T. performed co-immunoprecipitation analysis. K.T. and T.d.L. performed telomere fusion assays. D.D. provided information, reagents and advice. T.d.L. conceived the study and wrote the paper with input from all co-authors.

Competing interests D.D. is a founder of, owns equity in and receives funding from Repare Therapeutics.

Additional information
Extended data is available for this paper at https://doi.org/10.1038/s41586-018-0324-7.
Supplementary information is available for this paper at https://doi.org/10.1038/s41586-018-0324-7.
Reprints and permissions information is available at http://www.nature.com/reprints.
Correspondence and requests for materials should be addressed to T.L.
Publisher's note: Springer Nature remains neutral with regard to jurisdictional claims in published maps and institutional affiliations.

METHODS

No statistical methods were used to predetermine sample size. The experiments were not randomized and investigators were not blinded to allocation during experiments and outcome assessment.

Cell culture and expression constructs. *Brca1*$^{f/f}$ and *Trf2*$^{f/f}$*Lig4*$^{-/-}$ MEFs were derived from *Brca1*$^{f/f}$ mice[31], *Trf2*$^{f/f}$ mice[26] and *Lig4*$^{+/-}$ mice[32] by standard crosses. Mice were housed and cared for under Rockefeller University IACUC protocol 16865-H at the Rockefeller University's Comparative Bioscience Center, which provides animal care according to NIH guidelines. MEFs were isolated from embryonic-day 12.5 embryos and immortalized with pBabeSV40 large T antigen (a gift from G. Hannon) at early passage (P2/3), as previously described[26]. Genotypes were determined by Transnetyx, using real time PCR with allele-specific probes. *Tpp1*$^{f/f}$, *Tpp1*$^{f/f}$*53bp1*$^{-/-}$ (ref. [33]), *Tpp1*$^{f/f}$*Rif1*$^{f/f}$ or *Tpp1*$^{f/f}$*Rif1*$^{f/+}$ (ref. [20]) and *Pot1b*$^{Stop/Stop}$ (ref. [27]) MEFs have previously been described. MEFs and U2OS cells were cultured in Dulbecco's modified Eagle medium (DMEM, Corning) supplemented with 15% fetal bovine serum (FBS) (Gibco), non-essential amino acids (Gibco), 2 mM L-glutamine (Gibco), 100 U/ml penicillin, 100 μg/ml streptomycin (Gibco), 50 μM β-mercaptoethanol (Sigma). 293T, Phoenix and conditional *POT1*-knockout HT1080 clone c5[28] cells were cultured in DMEM supplemented with 10% bovine calf serum (BCS), non-essential amino acids, L-glutamine and penicillin–streptomycin as above. For most Cre-mediated gene deletion experiments (see exceptions below), retroviral infections with pMMP Hit & Run Cre were repeated three times[26]. Time points of cell collection indicate hours after the second Cre infection.

U2OS cells containing a LacO array and a tamoxifen- and Shield1-regulated mCherry–FOKI–LacI fusion were used as described[34]. Cells were collected 4 h after induction of FOKI by addition of 0.1 μM Shield1 and 10 μg/ml 4-OHT. Human *CTC1*$^{f/f}$ HCT116 cells[21] were cultured in McCoy's 5A supplemented with 10% FCS, non-essential amino acids, L-glutamine and penicillin–streptomycin as above. *CTC1* gene deletion was induced with 0.5 μM 4-OHT for 5 h. Gene deletion was confirmed by western blot using anti-CTC1 antibody (MABE1103, Millipore).

Mouse CTC1 tagged at the N terminus with a 6×Myc tag was delivered by retroviral transduction using pLPC or pWZL retroviral vectors. Human STN1 tagged at the N terminus with a 6×HA tag was delivered using the pLPC vector. Myc-tagged RPA32[35], and 53BP1 wild type and 53BP1ΔRif1[23] constructs were as described. Retroviral gene delivery was performed as described[16].

RNA depletion with shRNAs in pLKO.1 (Open Biosystems) was performed using the following shRNA target sites: shStn1 1: 5′-GATCCTGTGTTTCTAGCCTTT-3′ (TRCN0000180836, Sigma); shStn1 2: 5′-GCTGTCATCAGCGTGAAAGAA-3′ (TRCN0000184261, Sigma); shCtc1: 5′-CGGCAGATCACAGCATGATAA-3′; shAtr 1: 5′-CTGTGGTTGTATCTGTTCAAT-3′ (TRCN0000039613, Sigma); shAtr 2: 5′-GATGAACACATGGGATATTTA-3′ (TRCN0000196538, Sigma). Lentiviral constructs were co-transfected with packaging vectors into 293T cells and cells infected with the viral supernatant were selected in puromycin as described[16].

Drug treatments were as follows. ATR inhibition: 2.5 μM ETP-46464 (Sigma), 24 h; PARP1 inhibition: 0.1–10 μM Olaparib (Selleck Chemicals), 24 h; G2 arrest: 9 μM RO-3306 (Sigma), 12 h; polymerase α inhibition: 2.5 or 10 μM CD437 (Sigma) or 2 μM Aphidicolin, 4 h. ATM and ATR inhibition: 10 μM KU55933 (Selleck Chemical) with ATR inhibition as above for 4 h during induction of FOKI nuclease.

CRISPR–Cas9 gene disruption. Clonal cell lines with disruption of mouse 53BP1 were generated using Cas9 vector (Addgene) and sgRNA (sg53bp1 (2), 5′-GAGAATCTTCTATTATC-(PAM)-3′; sg53bp1 (3), 5′- GCATCTGCA GATTAGGA-(PAM)-3′[20]) delivered by nucleofection (Amaxa Kit R, Lonza). Clones were screened by immunoblotting and bi-allelic gene disruption was verified by Sanger sequencing of Topo-cloned PCR products of the relevant locus (sequences available on request). Clonal cell lines with mouse *Rev7* gene disruption were isolated similarly using the following sgRNAs: sgRev7(2), 5′-GTGTCCCCACCACAGTGG-(PAM)-3′; and sgRev7(3), 5′-GCCGGTTC AGGTGAGCCC-(PAM)-3′) (disrupted gene sequences available on request). Oligonucleotides were purchased from Sigma-Aldrich and cloned into the AflII-digested gRNA expression vector (Addgene) by Gibson Assembly (New England Biolabs). For isolation of populations with CRISPR–Cas9 disruption of mouse *Shld2* (FAM35A), 293T cells were transfected with lentiCrispr-v2-Shld2-sgRNA (5′- ATCAGTCAGATCCCTGCGTT-(PAM)-3′) or the vector control. The lentiviral supernatant was used for infection of *Tpp1*$^{f/f}$ or *Trf2*$^{f/f}$*Lig4*$^{-/-}$ MEFs; infections were done six times at 6–12 h intervals. Infected cells were then selected in puromycin for 3–5 days before Cre infection.

FOKI–LacI U2OS cells were infected with the 6×-HA-tagged human STN1 retrovirus and selected in puromycin. Subsequently, cells were subjected to lentiviral infection with lentiCrispr-v2 carrying sgRNA for human *53BP1*, *SHLD2* or *REV7* and selected in blasticidin for 3 days. Target sequences for gene disruption are as follows: human *53BP1* sgRNA1 (5′-CAGAATCATCCTCTAGAACC-(PAM)-3′), *53BP1* sgRNA2 (5′-TTGATCTCACTTGTGATTCG-(PAM)-3′), *SHLD2* sgRNA1 (5′-TCTGGAGAACCAATAGATTC-(PAM)-3′), *SHLD2* sgRNA2 (5′-TTTGAGCTAAAAAAGCAACC-(PAM)-3′), *REV7* sgRNA1 (5′-CCT CAACTTTGGCCAAGGTA-(PAM)-3′), *REV7* sgRNA2 (5′-TATACTGATTC AGCTCCGGG-(PAM)-3′). For each gene the two sgRNAs were either used individually or together.

In-gel analysis of single-stranded telomeric DNA. Mouse telomeric overhang and telomeric restriction fragment patterns were analysed 96–120 h after Cre treatment by in-gel hybridization with a γ-^{32}P-ATP end-labelled $(AACCCT)_4$ probe, as previously described[26]. Treatment with *E. coli* exonuclease I before MboI digestion was used to verify the 3′ terminal position of the single-stranded DNA as previously described[20]. ImageQuant software was used to quantify the single-stranded telomere overhang signals and the signal from total telomeric DNA in the same lane in the denatured gel. In each experiment, this ratio was set to 1 for lanes not treated with Cre or shRNA and the ratios for the treated samples are given relative to this control.

Flow cytometry. FACS was performed as previously described[36] with gating.

Immunoblotting. Immunoblotting was performed as described[16] with the following antibodies: 53BP1 (175933, Abcam; NB100-304, Novus Biological); ATR (sc-1887, Santa Cruz Biotechnology); BRCA1 (MAB22101, R+D systems); CHK1 (sc-8408, Santa Cruz Biotechnology); CHK1-S345-P (#2341S; Cell Signaling Technology); CHK2 (BD 611570, BD Biosciences); Flag-tag (M2, Sigma; F1804, Sigma); γ-tubulin (GTU488, Sigma); MAD2L2/REV7 (ab180579, Abcam); Myc-tag (9B11, Cell Signaling Technology); OBFC1/STN1 (E10-376450, Santa Cruz Biotechnology); Tagged TEN1 was not detectable by immunoblotting of transfected 293T cells.

For detection of RPA phosphorylation, conditional *CTC1* HCT116 cells or MEFs were irradiated and collected 3 h later. Cells were washed in PBS, and then collected by scraping in Laemmli sample buffer, boiling for 5 min and shearing through a syringe. Proteins were separated by SDS–PAGE on 8–16% Tris-glycine gradient gels (Invitrogen), and transferred to nitrocellulose overnight. Immunoblotting for pRPA followed standard protocols with blocking in 5% milk/TBST and the pRPA antibody (S4/S8; Bethyl) diluted 1:1,000 in 1% milk/TBST.

Immunoprecipitation. Immunoprecipitation was carried out as described[16]. The following plasmids were used: pLPC-flag-POT1a and pLPC-flag-POT1b[27]; pLPC-myc-mouse Ctc1, pLPC-myc-mouse Stn1 and pLPC-myc-mouse Ten1[16]; pLPC-myc-human Ctc1, pLPC-myc-human Stn1, pLPC-myc-human Ten1, pCD-NA5-flag-human Shld1 (C20orf196) and pLPC-myc-hRev7, pLPC-flag-mouse Shld1 (orthologue of C20orf196). Human *REV7*, *SHLD1*, *CTC1*, *STN1* and *TEN1* ORFs were generated by PCR and mouse *Shld1* was generated by RT–PCR. Co-transfection of *Shld1* and *Rev7* with CST in 293T cells was performed using calcium phosphate co-precipitation. Lysates were prepared in lysis buffer containing 50 mM Tris-HCl (pH 7.4), 150 mM NaCl, 10% glycerol and 0.1% NP-40, Complete protease inhibitor mix (Roche), and PhosSTOP phosphatase inhibitor mix (Roche) and 50 U benzonase.

Yeast two-hybrid assays. For yeast two-hybrid analysis, full-length versions of human CST and shieldin components were cloned into the NdeI site of the pGBKT7 and pGADT7 vectors (Clontech). Plasmids in the indicated pairwise combinations were co-transformed into budding yeast strain PJ69-4A (*MATa trp1-901 leu2-3,112 ura3-52 his3-200 gal4 gal80 LYS2::GAL1-HIS3 GAL2-ADE2 met2::GAL7-lacZ*) and selected on synthetic complete drop-out medium lacking tryptophan and leucine. Protein interactions were tested by plating on the same medium but also lacking adenine.

Immunofluorescence and IF–FISH. Previously published procedures were followed for immunofluorescence and IF–FISH[16]. Immunofluorescence for Myc-tagged RPA32 or CTC1 (mouse monoclonal, 9B11 or rabbit monoclonal, 71D10, Cell Signaling Technology), HA-tagged STN1 (3724, Cell Signaling Technology), endogenous Polα (sc-137021, Santa Cruz), and 53BP1 (612522, BD Biosciences) was carried out using the cytoskeleton extraction protocol[37]. Intensity measurements of RPA32–Myc immunofluorescence were performed in FIJI as follows: nuclei were identified using thresholding, segmented and identified as regions of interest. The average image background was then subtracted from the image, and the total raw pixel intensity within each area of interest in the channel of interest was calculated. RAD51 (70-001, Bioacademia), and γH2AX (05636, Millipore) were detected in cells fixed in 3% PFA, and foci showing co-localization of RAD51 with γH2AX were quantified. Immunofluorescence imaging was performed on a Zeiss Axioplan II microscope equipped with a Hamamatsu C4742-95 camera using Volocity software or on a DeltaVision (Applied Precision) equipped with a cooled charge-coupled device camera (DV Elite CMOS Camera), a PlanApo 60× 1.42 NA objective or 100× 1.40 NA objective (Olympus America), and SoftWoRx software.

Telomere fusion assays. SV40LT-immortalized *Trf2*$^{f/f}$*Rosa*^{creER} cells were infected with *Stn1* shRNA (or the empty vector) and 24 h later Cre was induced for 24 h with 4-OHT. Cells were collected, counted (to rule out a proliferation defect) and processed for telomeric FISH on metaphases 72 h after Cre induction. This early time point was selected to avoid any effect of the *Stn1* shRNA on proliferation, as

diminished proliferation reduces fusion frequencies. Telomere fusions were scored as previously described[26].

Survival assays and chromosome analysis. PARPi survival assays and analysis of misrejoined chromosomes were carried out as described[19], except that for analysis of radial chromosomes, MEFs were incubated with 0.5 μM Olaparib (AZD2281) for 24 h before collection. For the survival assays, MEFs were seeded in 6-well plates in duplicate at 10, 50, 100, 500, 1,000, 5,000 or 10,000 cells per well. After 24 h, cells were treated with Olaparib at the indicated concentrations for 24 h. Cells were then provided with medium without Olaparib and incubated for one week with a medium change at day 4. Colonies were fixed and stained with 50% methanol, 2% methylene blue, rinsed with water and dried before counting. The survival percentage at each PARPi concentration compared to untreated cells was calculated using wells with 10–100 colonies. Two technical replicates at two cell concentrations were scored for each condition in three independent experiments.

Reporting summary. Further information on experimental design is available in the Nature Research Reporting Summary linked to this paper.

Data availability. All data that were generated and/or analysed in this study are included in the published paper and its Supplementary Information.

31. Xu, X. et al. Centrosome amplification and a defective G2-M cell cycle checkpoint induce genetic instability in BRCA1 exon 11 isoform-deficient cells. *Mol. Cell* **3**, 389–395 (1999).
32. Frank, K. M. et al. Late embryonic lethality and impaired V(D)J recombination in mice lacking DNA ligase IV. *Nature* **396**, 173–177 (1998).
33. Kibe, T., Osawa, G. A., Keegan, C. E. & de Lange, T. Telomere protection by TPP1 is mediated by POT1a and POT1b. *Mol. Cell. Biol.* **30**, 1059–1066 (2010).
34. Tang, J. et al. Acetylation limits 53BP1 association with damaged chromatin to promote homologous recombination. *Nat. Struct. Mol. Biol.* **20**, 317–325 (2013).
35. Gong, Y., Handa, N., Kowalczykowski, S. C. & de Lange, T. PHF11 promotes DSB resection, ATR signaling, and HR. *Genes Dev.* **31**, 46–58 (2017).
36. Takai, H., Wang, R. C., Takai, K. K., Yang, H. & de Lange, T. Tel2 regulates the stability of PI3K-related protein kinases. *Cell* **131**, 1248–1259 (2007).
37. Mirzoeva, O. K. & Petrini, J. H. DNA damage-dependent nuclear dynamics of the Mre11 complex. *Mol. Cell. Biol.* **21**, 281–288 (2001).

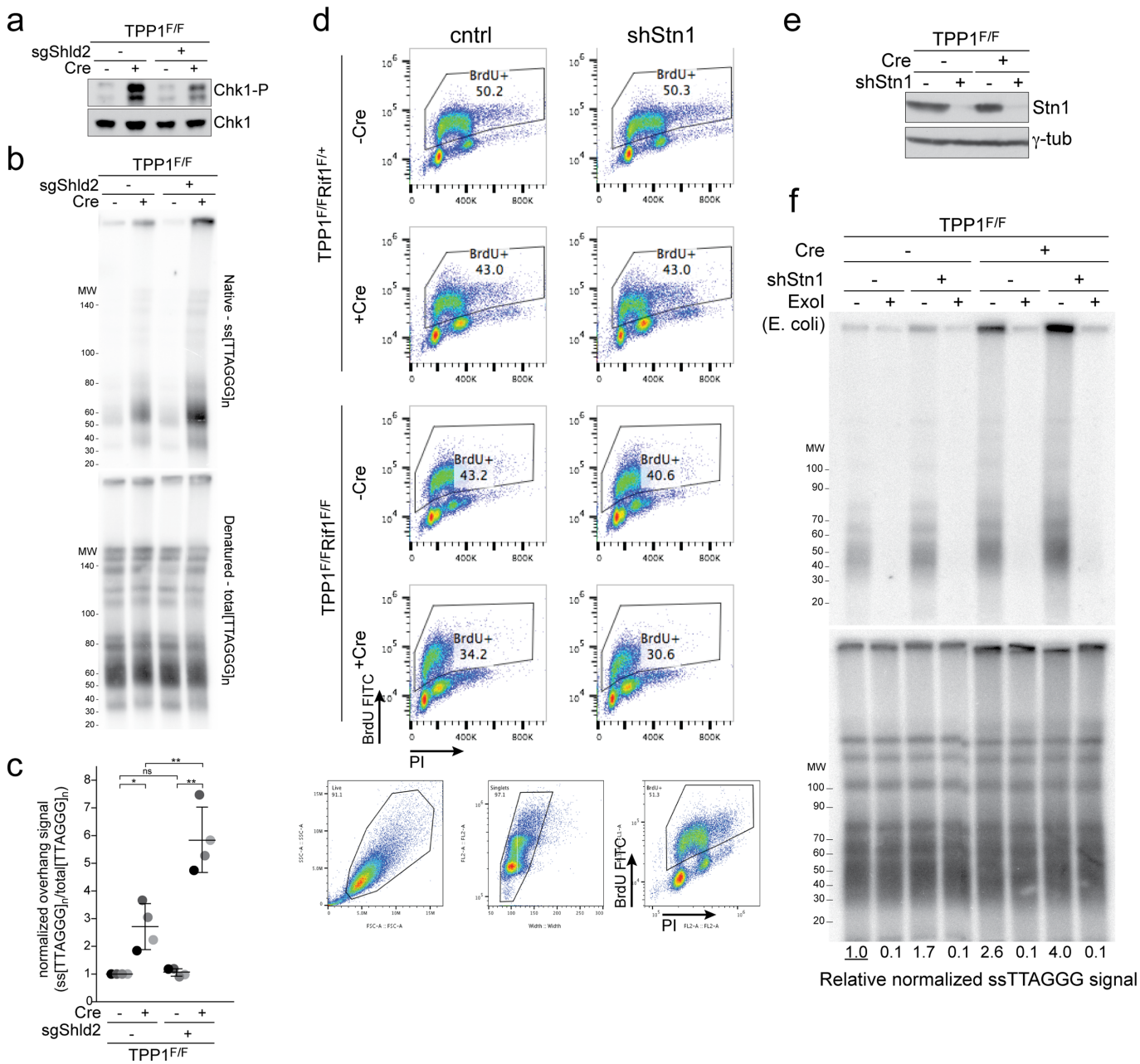

Extended Data Fig. 1 | Shieldin and CST counteract telomere hyper-resection. a-c, Effect of SHLD2 on hyper-resection at telomeres that lack TPP1. **a**, Immunoblot for CHK1-P, an indicator of TPP1 deletion, in *Tpp1*$^{f/f}$ MEFs with and without bulk population treatment with a *Shld2* sgRNA and/or Cre (representative of three experiments). **b**, Quantitative analysis of telomere end resection as in Fig. 1c using the cells shown in **a**. **c**, Quantification of the extent of resection detected in **b**, as in Fig. 1d. Mean (centre bars) and s.d. (error bars) from four independent experiments. *$P < 0.05$, **$P < 0.01$, two-tailed Welch's *t*-test. **d**, Fluorescence-activated cell sorting (FACS) profiles of the indicated cells incubated with BrdU to measure S phase effects of the *Stn1* shRNA. Gating strategy for live cells and singlets is shown below the FACS profiles. Representative of two experiments. **e**, **f**, Experiments to verify that the single-stranded DNA signal derives from a 3′ overhang. **e**, Immunoblot for STN1 and γ-tubulin in *Tpp1*$^{f/f}$ (*Rif1*$^{f/+}$) cells treated with *Stn1* shRNA and/or Cre. Representative of two experiments. **f**, Quantitative assay for telomeric overhangs, as in Fig. 1c. Plugs in the ExoI lanes were treated with the 3′ exonuclease from *E. coli*. Representative of two experiments.

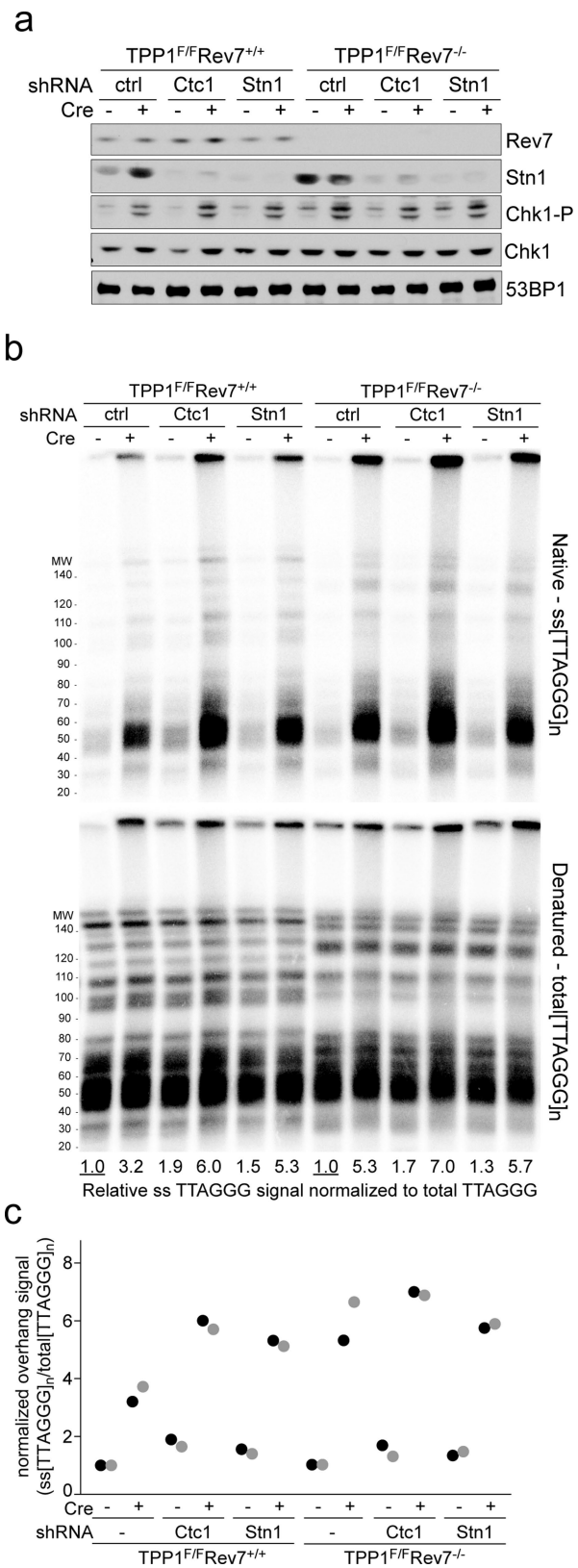

Extended Data Fig. 2 | Hyper-resection at telomeres that lack TPP1 is counteracted by CST and shieldin. a, Immunoblots showing absence of REV7 and reduction of STN1 expression in the indicated *Tpp1*$^{f/f}$ and *Tpp1*$^{f/f}$*Rev7*$^{-/-}$ MEFs treated with either *Ctc1* or *Stn1* shRNA. Diminished STN1 expression is used as a proxy for the efficacy of the *Ctc1* shRNA. Representative of two experiments. **b**, Quantitative analysis of telomeric overhangs, as in Fig. 1c. Representative of two experiments. **c**, Quantification of the effect of *Ctc1* and *Stn1* shRNA on resection at telomeres that lack TPP1, as in Fig. 1d. Data are obtained from two independent REV7-proficient and two independent REV7-deficient clones (light and dark shading).

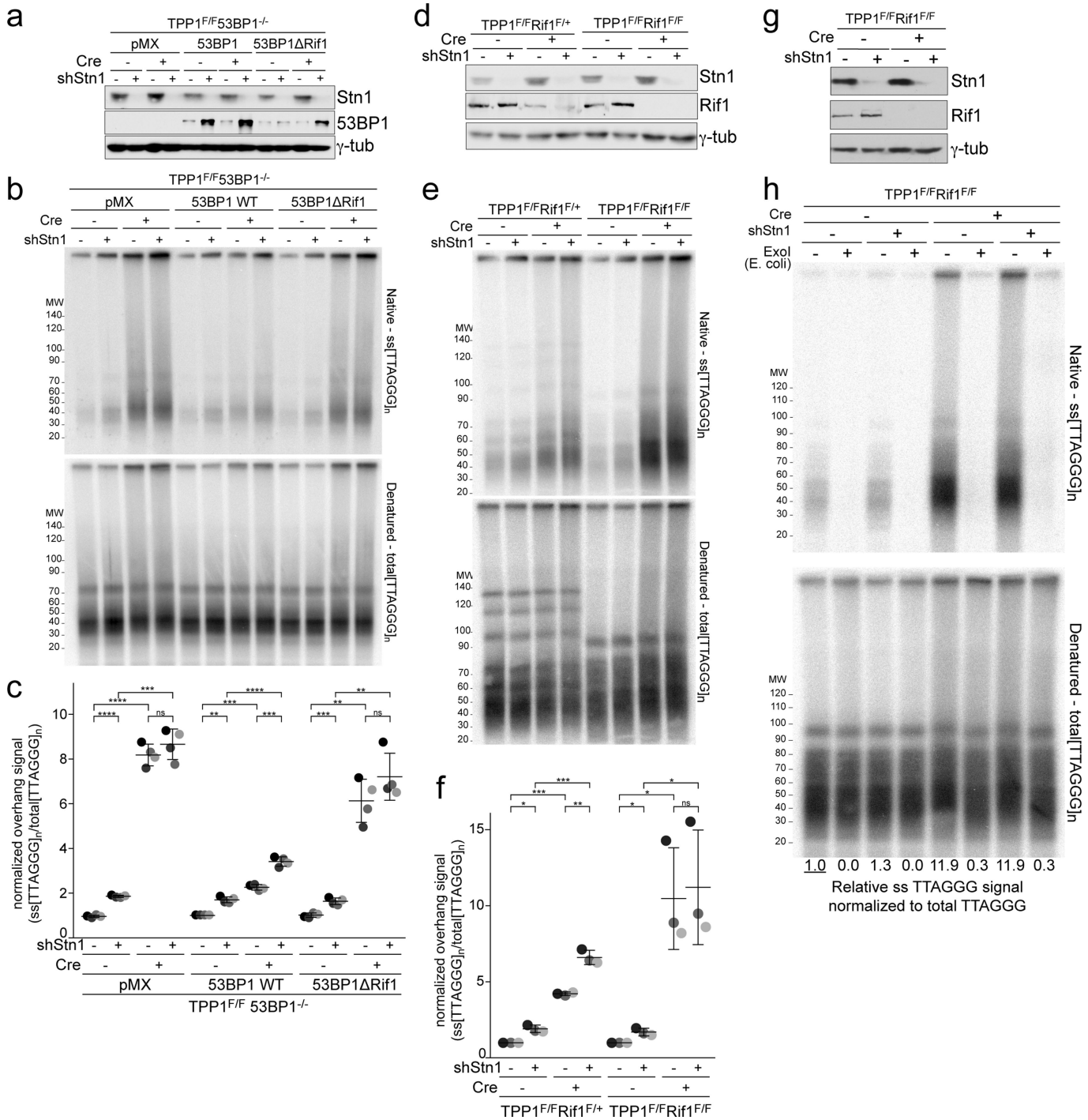

Extended Data Fig. 3 | No effect of CST depletion on telomere hyper-resection when 53BP1 or RIF1 are absent. a, SV40LT-immortalized *Tpp1*$^{f/f}$*53bp1*$^{-/-}$ cells were complemented with wild-type 53BP1 or a mutant 53BP1 that lacks the ability to interact with RIF1, treated with a *Stn1* shRNA as indicated and analysed by immunoblotting for 53BP1 and STN1. Representative of four experiments. **b**, Quantitative analysis of telomeric overhangs, as in Fig. 1c. **c**, Quantification of the resection at telomeres that lack TPP1, in four independent experiments performed as in Fig. 1d. **d**, Immunoblots showing loss of RIF1 and STN1 in the indicated *Tpp1*$^{f/f}$*Rif1*$^{f/+}$ and *Tpp1*$^{f/f}$*Rif1*$^{f/f}$ MEFs treated with Cre (96 h) as indicated, and with or without *Stn1* shRNA. Note the diminished levels of RIF1 after Cre, owing to heterozygosity in the *Tpp1*$^{f/f}$*Rif1*$^{f/+}$ cells. **e**, Quantitative analysis of telomeric overhangs, as in Fig. 1c. **f**, Quantification of the extent of resection detected, as in **e**, determined from three independent experiments (indicated by different shades of grey) showing mean (centre bars) and s.d. (error bars). Each experiment involved all indicated samples analysed in parallel. **g, h**, Experiments to verify that the single-stranded DNA signal derives from a 3′ overhang. **g**, Immunoblot for STN1 and γ-tubulin in *Tpp1*$^{f/f}$*Rif1*$^{f/f}$ cells treated with *Stn1* shRNA and/or Cre. Representative of two experiments. **h**, Quantitative assay for telomeric overhangs, as in Fig. 1c. Plugs in the ExoI lanes were treated with the 3′ exonuclease from *E. coli*. Representative of two experiments. *$P < 0.05$, **$P < 0.01$, ***$P < 0.001$, ****$P < 0.0001$, two-tailed Welch's *t*-test.

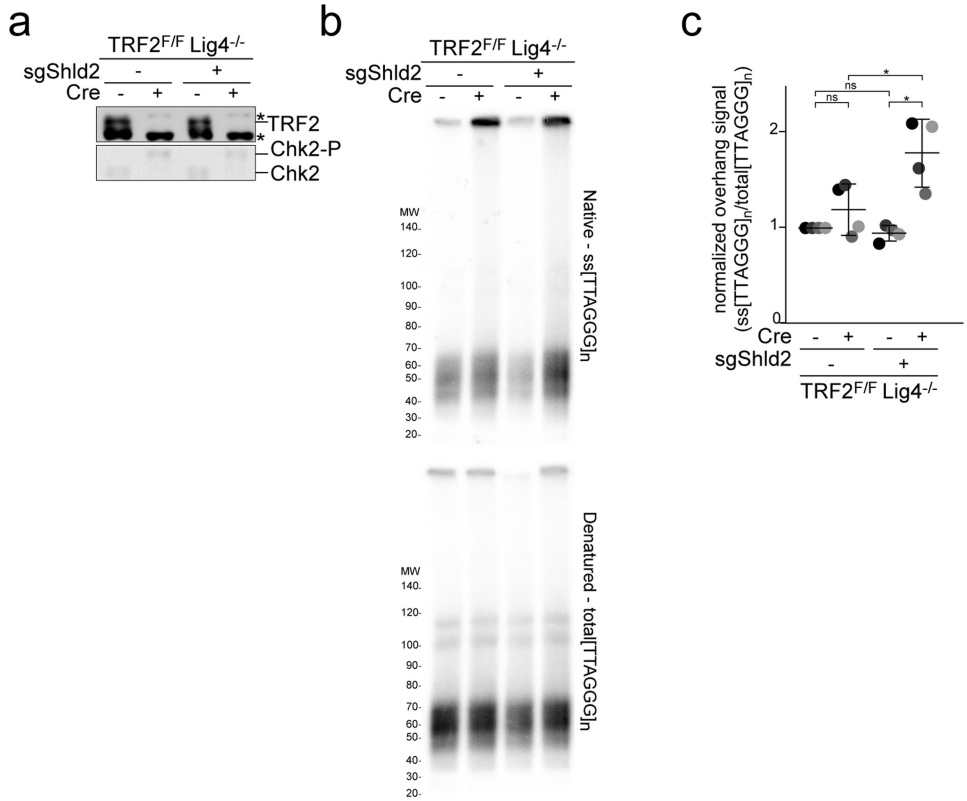

Extended Data Fig. 4 | SHLD2 counteracts resection at telomeres that lack TRF2. a, Immunoblots for TRF2 deletion and CHK2 phosphorylation in *Trf2*$^{f/f}$*Lig4*$^{-/-}$ MEFs, with and without bulk population treatment with a *Shld2* sgRNA and/or Cre. Asterisk, non-specific band. Representative of three experiments. **b**, Quantitative analysis of telomere end resection, as in Fig. 1c, using the cells shown in **a**. **c**, Quantification of the extent of resection detected in **b**, as in Fig. 1d. Mean (centre bars) and s.d. (error bars) from four independent experiments. *$P < 0.05$, two-tailed Welch's *t*-test.

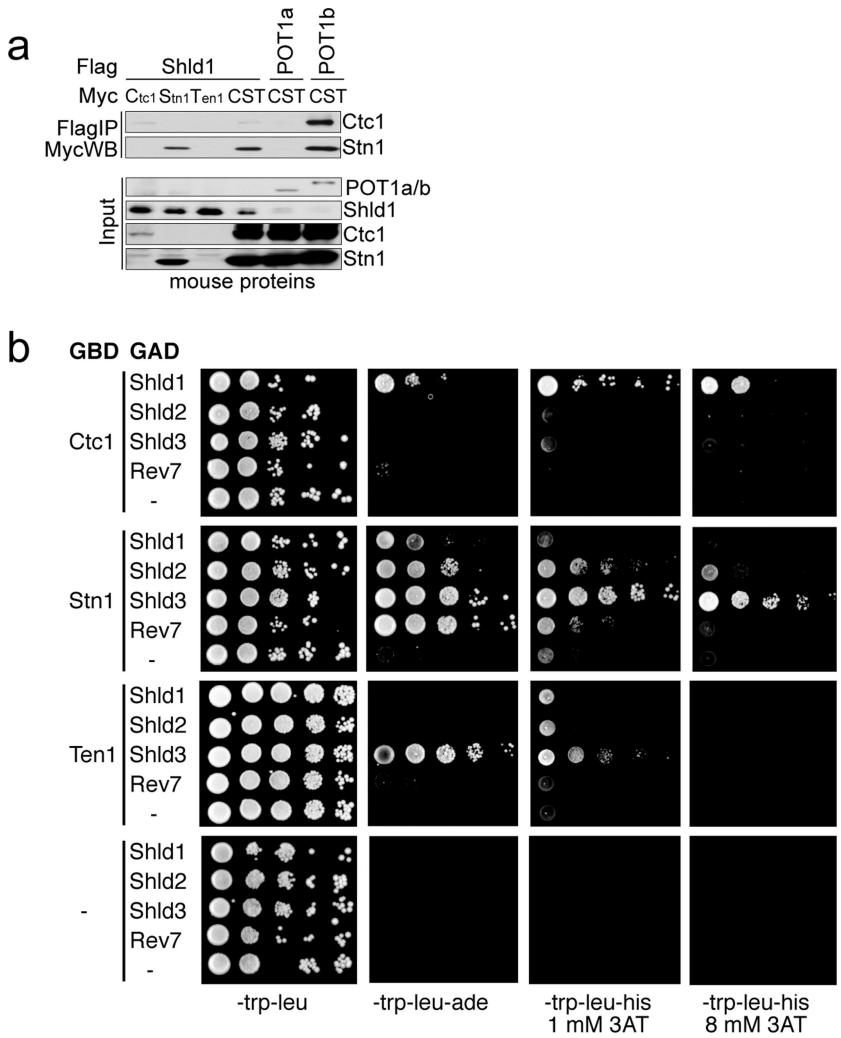

Extended Data Fig. 5 | CST interacts with shieldin. a, Immunoprecipitation of individual mouse CST subunits or the three subunit complex (each subunit bearing a Myc tag) with Flag-tagged mouse SHLD1, co-expressed in 293T cells. Flag-tagged POT1B and POT1A serve as positive and negative controls for CST binding, respectively. Representative of two experiments. **b**, Two-hybrid analysis of CST-shieldin interaction. Yeast cultures were grown overnight in synthetic complete medium that lacked tryptophan and leucine, to a density of 5×10^7 cells per millilitre. Serial tenfold dilutions were generated and 4 μl of each dilution was spotted on synthetic complete medium that lacked the nutrients tryptophan, leucine, adenine and histidine, and contained 3-aminotriazole (3-AT), as indicated. Plates were then incubated for 5 days at 30 °C before imaging. Representative of three experiments.

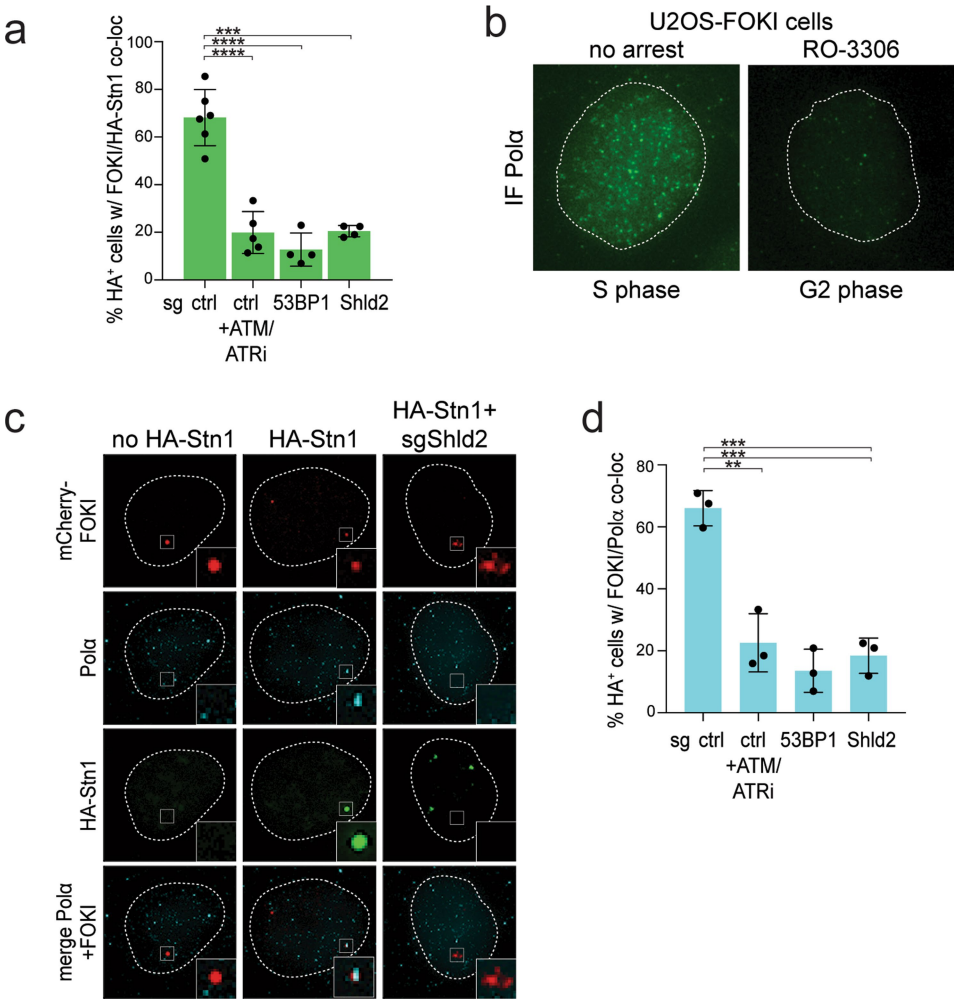

Extended Data Fig. 6 | Localization of CST and Polα to DSBs. **a**, Quantification of HA–STN1 localization to DSBs induced by FOKI, as in Fig. 3e. Mean (centre bars) and s.d. (error bars) from 4–6 independent experiments, with >80 induced nuclei for each condition in each experiment. **b**, Immunofluorescence for endogenous Polα in FOKI–LacI U2OS cells in S phase and after RO3306 treatment (G2). Dotted lines denote the outline of the nucleus. Representative of two experiments. **c**, Examples of HA–STN1 and Polα localization at DSBs induced by FOKI in G2-arrested FOKI–LacI U2OS cells (as in Fig. 3f). Representative of three experiments. **d**, Quantification of co-localization of Polα with DSBs induced by FOKI (as in Fig. 3f). Mean (centre bars) and s.d. (error bars) from three independent experiments, with >80 induced nuclei for each condition in each experiment. $^{**}P < 0.01$, $^{***}P < 0.001$, $^{****}P < 0.0001$, two-tailed Welch's *t*-test.

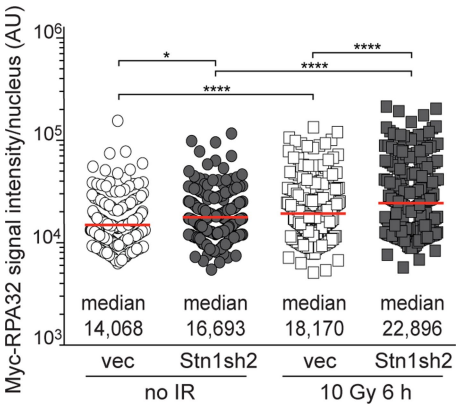

Extended Data Fig. 7 | Effect of STN1 knockdown on the intensity of RPA foci induced by ionizing radiation. Quantification of Myc–RPA32 intensity per nucleus in the experiments shown in Fig. 3g, h. Medians (centre bars and numbers below) obtained from four independent experiments, with >20 nuclei for each experimental condition in each experiment. Each symbol represents one nucleus. *$P < 0.05$, ****$P < 0.0001$, two-tailed Welch's t-test.

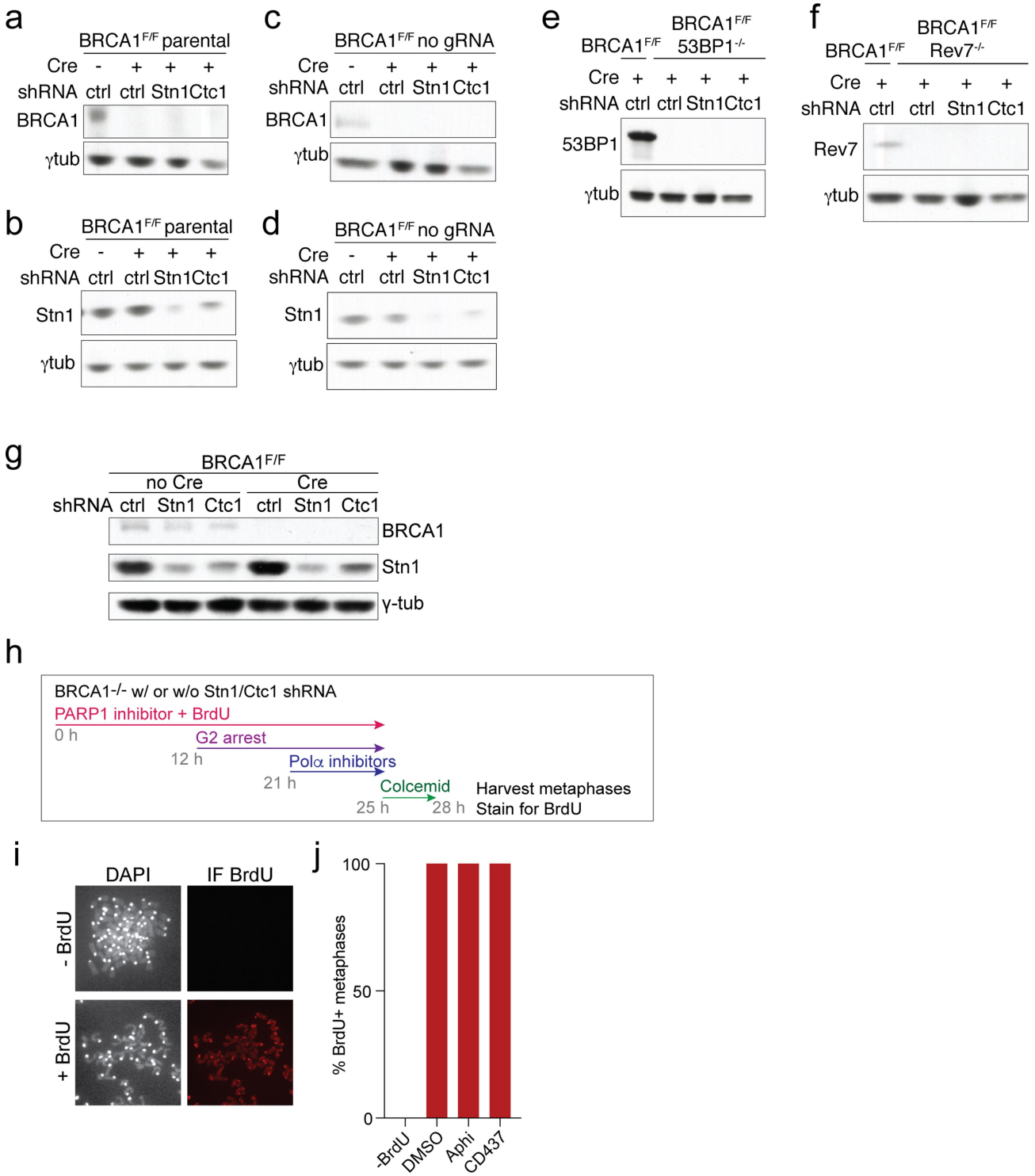

Extended Data Fig. 8 | Effect of CST and Polα on PARPi treatment of BRCA1-deficient cells. a–f, Immunoblots on the MEFs used in Fig. 4a–e to verify the absence of deleted proteins and efficacy of the shRNAs. Reduction in STN1 expression is used as a proxy for the efficacy of the *Ctc1* shRNA because no antibody to mouse CTC1 is available. Each immunoblot is representative of three experiments. **g**, Immunoblots for BRCA1 and STN1 in the cells used in Fig. 4f. Representative of two experiments. **h–j**, Control experiment to assess that cells analysed in Fig. 4f progressed through S phase during treatment with PARPi. **h**, Experimental timeline, as in Fig. 4f, but with inclusion of BrdU in the medium during treatment with PARPi. **i**, Example of the assay for the presence of BrdU (immunofluorescence) in metaphases collected after the experimental timeline, as in **h**. **j**, Quantification of the BrdU incorporation into metaphase chromosomes, as in **i** (one experiment with ten metaphases per condition).

nature research

Corresponding author(s): Titia de Lange

Reporting Summary

Nature Research wishes to improve the reproducibility of the work that we publish. This form provides structure for consistency and transparency in reporting. For further information on Nature Research policies, see Authors & Referees and the Editorial Policy Checklist.

Statistical parameters

When statistical analyses are reported, confirm that the following items are present in the relevant location (e.g. figure legend, table legend, main text, or Methods section).

n/a	Confirmed	
☐	☒	The exact sample size (*n*) for each experimental group/condition, given as a discrete number and unit of measurement
☐	☒	An indication of whether measurements were taken from distinct samples or whether the same sample was measured repeatedly
☐	☒	The statistical test(s) used AND whether they are one- or two-sided *Only common tests should be described solely by name; describe more complex techniques in the Methods section.*
☒	☐	A description of all covariates tested
☒	☐	A description of any assumptions or corrections, such as tests of normality and adjustment for multiple comparisons
☐	☒	A full description of the statistics including central tendency (e.g. means) or other basic estimates (e.g. regression coefficient) AND variation (e.g. standard deviation) or associated estimates of uncertainty (e.g. confidence intervals)
☒	☐	For null hypothesis testing, the test statistic (e.g. *F*, *t*, *r*) with confidence intervals, effect sizes, degrees of freedom and *P* value noted *Give P values as exact values whenever suitable.*
☒	☐	For Bayesian analysis, information on the choice of priors and Markov chain Monte Carlo settings
☒	☐	For hierarchical and complex designs, identification of the appropriate level for tests and full reporting of outcomes
☒	☐	Estimates of effect sizes (e.g. Cohen's *d*, Pearson's *r*), indicating how they were calculated
☐	☒	Clearly defined error bars *State explicitly what error bars represent (e.g. SD, SE, CI)*

Our web collection on statistics for biologists may be useful.

Software and code

Policy information about availability of computer code

Data collection	FIJI, Volocity, Prism, R, Microsoft Excel, ImageQuant, SoftWoRx, Zifit, CELL Quest Software, FloJo
Data analysis	FIJI, Volocity, Prism, R, Microsoft Excel, ImageQuant, SoftWoRx, Zifit, CELL Quest Software, FloJo, ImageJ

For manuscripts utilizing custom algorithms or software that are central to the research but not yet described in published literature, software must be made available to editors/reviewers upon request. We strongly encourage code deposition in a community repository (e.g. GitHub). See the Nature Research guidelines for submitting code & software for further information.

Data

Policy information about availability of data

All manuscripts must include a data availability statement. This statement should provide the following information, where applicable:

- Accession codes, unique identifiers, or web links for publicly available datasets
- A list of figures that have associated raw data
- A description of any restrictions on data availability

Provide your data availability statement here.

Field-specific reporting

Please select the best fit for your research. If you are not sure, read the appropriate sections before making your selection.

☒ Life sciences ☐ Behavioural & social sciences

For a reference copy of the document with all sections, see nature.com/authors/policies/ReportingSummary-flat.pdf

Life sciences

Study design

All studies must disclose on these points even when the disclosure is negative.

Sample size	Sample size was determined based on prior published data from similar experiments (including data from our lab).
Data exclusions	No data was excluded with the exception of data from failed experiments (e.g. sample loss; failure of Cre-mediated deletion; cell culture anomalies).
Replication	Every experiment reported was done at least three times with consistent results.
Randomization	We report on in vitro experiments where randomization is not required. However, all experiments were done in a 'randomized' fashion in the sense that random culture dishes containing the same cell population were chosen for the various biological perturbations (e.g. treatment with Cre, or not; IR or no radiation; infection with shRNA vectors).
Blinding	We report on in vitro experiments where blinding is not required. However, blinding of samples was performed before scoring data where possible (e.g. scoring of co-localization of IF signals). In experiments where the results immediately revealed the experimental setting (e.g. assays for telomeric overhang; immunoblots for pRPA) scoring was not done blinded.

Materials & experimental systems

Policy information about availability of materials

n/a	Involved in the study
☐	☒ Unique materials
☐	☒ Antibodies
☐	☒ Eukaryotic cell lines
☐	☐ Research animals
☐	☐ Human research participants

Unique materials

Obtaining unique materials	Materials are available upon request (see http://delangelab.rockefeller.edu). Shelterin subunit knockout mice generated in our lab have been deposited at The Jackson Laboratory. Conditional shelterin subunit KO MEFs have been deposited at the ATCC. De Lange lab constructs have been deposited at Addgene. Protocols are available at http://delangelab.rockefeller.edu.

Antibodies

Antibodies used	Immunoblotting: 53BP1 (175933, Abcam; NB100-304, Novus Biological); ATR (sc-1887, Santa Cruz Biotechnology); BRCA1 (MAB22101, R+D systems); Chk1 (sc-8408, Santa Cruz Biotechnology); Chk1-S345-P (#2341S; Cell Signaling Technology); Chk2 (BD 611570, BD Biosciences); flag-tag (M2, Sigma; F1804, Sigma); γtubulin (GTU488, Sigma); MAD2L2/Rev7 (ab180579, Abcam); myc-tag (9B11, Cell Signaling Technology); OBFC1/Stn1 (E10-376450, Santa Cruz Biotechnology); pRPA (S4/S8; Bethyl); human CTC1 (MABE1103, Millipore). IF: Myc-RPA32 or Myc-Ctc1 (mouse monoclonal, 9B11 or rabbit monoclonal, 71D10, Cell Signaling Technology); HA-tagged Stn1 (3724, Cell Signaling Technology); Polα (sc-137021, Santa Cruz); 53BP1 (612522, BD Biosciences); Rad51 (70-001, Bioacademia); γH2AX (05636, Millipore).
Validation	Where possible, antibodies were validated by comparing wild-type cells to KO cells by western blot and/or immunofluorescence.

Eukaryotic cell lines

Policy information about cell lines

Cell line source(s)	BRCA1F/F MEFs were derived from BRCA1F/F mice Xu, X., Weaver, Z., Linke, S. P., Li, C., Gotay, J., Wang, X. W., Harris, C. C., Ried, T. & Deng, C. X. Centrosome amplification and a defective G2-M cell cycle checkpoint induce genetic instability in BRCA1 exon 11 isoform-deficient cells. Mol Cell 3, 389-95. (1999). TRF2F/F Lig4-/- MEFs were derived from TRF2F/F and Lig4+/- mice by standard crosses (TRF2: Celli, G. B. & de Lange, T. DNA

processing is not required for ATM-mediated telomere damage response after TRF2 deletion. Nat Cell Biol 7, 712-718 (2005); Lig4: Frank, K. M., Sekiguchi, J. M., Seidl, K. J., Swat, W., Rathbun, G. A., Cheng, H. L., Davidson, L., Kangaloo, L. & Alt, F. W. Late embryonic lethality and impaired V(D)J recombination in mice lacking DNA ligase IV. Nature 396, 173-7. (1998).
TPP1F/F MEFs were available in our lab and were previously described (Kibe, T., Osawa, G. A., Keegan, C. E. & de Lange, T. Telomere Protection by TPP1 Is Mediated by POT1a and POT1b. Mol Cell Biol 30, 1059-1066 (2010);
TPP1F/F 53BP1-/- , TPP1F/F Rif1F/F or Rif1F/+ MEFs were available in our lab and were previously described (Kibe, T., Zimmermann, M. & de Lange, T. TPP1 Blocks an ATR-Mediated Resection Mechanism at Telomeres. Mol Cell 61, 236-246 (2016).);
POTbSTOP/STOP (referred to as POT1b-/-) MEFs were available in our lab and were previously described (Hockemeyer, D., Daniels, J. P., Takai, H. & de Lange, T. Recent expansion of the telomeric complex in rodents: Two distinct POT1 proteins protect mouse telomeres. Cell 126, 63-77 (2006));
U2OS cells containing a LacO array and a tamoxifen- and Shield1-regulated mCherry-FOKI-LacI fusion were described and provided by Dr. Greenberg (Tang, J., Cho, N. W., Cui, G., Manion, E. M., Shanbhag, N. M., Botuyan, M. V., Mer, G. & Greenberg, R. A. Acetylation limits 53BP1 association with damaged chromatin to promote homologous recombination. Nat Struct Mol Biol 20, 317-325 (2013));
Human conditional CTC1 KO HCT116 cells were described and provide by Dr. Price (Feng, X., Hsu, S. J., Kasbek, C., Chaiken, M. & Price, C. M. CTC1-mediated C-strand fill-in is an essential step in telomere length maintenance. Nucleic Acids Res 45, 4281-4293 (2017)).
POT1 knockout HT1080 clone c5 cells were available in our lab and were previously described (Takai, H., Jenkinson, E., Kabir, S., Babul-Hirji, R., Najm-Tehrani, N., Chitayat, D. A., Crow, Y. J. & de Lange, T. A POT1 mutation implicates defective telomere end fill-in and telomere truncations in Coats plus. Genes Dev 30, 812-826 (2016).).

Authentication

All MEF cell lines were genotyped by Transnetyx Inc. using real time PCR with allele-specific probes and confirmed by western blot. The three human cell lines were verified based on the appropriate cell biological read-outs (Cre induced loss of Ctc1 or POT1 and induction of FOKI cuts).

Mycoplasma contamination

No mycoplasma contaminations were found in the course of these experiments.

Commonly misidentified lines
(See ICLAC register)

No commonly misidentified cell lines were used in this study.

Research animals

Policy information about studies involving animals; ARRIVE guidelines recommended for reporting animal research

Animals/animal-derived materials

Pregnant female mice were used to isolate MEFs from E12.5 embryos. Species Mus musculus musculus; Strain mixed C57BL/6 and 129 ; sex female and male; age range 2-6 months. Mice were housed and cared for under the Rockefeller University AIACUC protocol 16865-H at the Rockefeller University's Comparative Bioscience Center, which provides animal care according to NIH guidelines.

Human research participants

Policy information about studies involving human research participants

Population characteristics

Describe the covariate-relevant population characteristics of the human research participants (e.g. age, gender, genotypic information, past and current diagnosis and treatment categories).

Method-specific reporting

n/a	Involved in the study
☐	☐ ChIP-seq
☐	☒ Flow cytometry
☐	☐ Magnetic resonance imaging

ChIP-seq

Data deposition

☐ Confirm that both raw and final processed data have been deposited in a public database such as GEO.

☐ Confirm that you have deposited or provided access to graph files (e.g. BED files) for the called peaks.

Data access links
May remain private before publication.

For "Initial submission" or "Revised version" documents, provide reviewer access links. For your "Final submission" document, provide a link to the deposited data.

Files in database submission

Provide a list of all files available in the database submission.

Genome browser session
(e.g. UCSC)

Provide a link to an anonymized genome browser session for "Initial submission" and "Revised version" documents only, to enable peer review. Write "no longer applicable" for "Final submission" documents.

Methodology

Replicates	*Describe the experimental replicates, specifying number, type and replicate agreement.*
Sequencing depth	*Describe the sequencing depth for each experiment, providing the total number of reads, uniquely mapped reads, length of reads and whether they were paired- or single-end.*
Antibodies	*Describe the antibodies used for the ChIP-seq experiments; as applicable, provide supplier name, catalog number, clone name, and lot number.*
Peak calling parameters	*Specify the command line program and parameters used for read mapping and peak calling, including the ChIP, control and index files used.*
Data quality	*Describe the methods used to ensure data quality in full detail, including how many peaks are at FDR 5% and above 5-fold enrichment.*
Software	*Describe the software used to collect and analyze the ChIP-seq data. For custom code that has been deposited into a community repository, provide accession details.*

Flow Cytometry

Plots

Confirm that:

☒ The axis labels state the marker and fluorochrome used (e.g. CD4-FITC).

☒ The axis scales are clearly visible. Include numbers along axes only for bottom left plot of group (a 'group' is an analysis of identical markers).

☒ All plots are contour plots with outliers or pseudocolor plots.

☒ A numerical value for number of cells or percentage (with statistics) is provided.

Methodology

Sample preparation	FACS was performed as previously described (Takai et al., Mol Cell 2007)
Instrument	BD LSR II or BD Accuri C6
Software	CELL Quest Software (Becton Dickinson) or FlowJo.
Cell population abundance	n/a
Gating strategy	Gating was performed as shown in Extended Data Fig. 1. Standard gating was applied based on FSC/SSC data.

☐ Tick this box to confirm that a figure exemplifying the gating strategy is provided in the Supplementary Information.

Magnetic resonance imaging

Experimental design

Design type	*Indicate task or resting state; event-related or block design.*
Design specifications	*Specify the number of blocks, trials or experimental units per session and/or subject, and specify the length of each trial or block (if trials are blocked) and interval between trials.*
Behavioral performance measures	*State number and/or type of variables recorded (e.g. correct button press, response time) and what statistics were used to establish that the subjects were performing the task as expected (e.g. mean, range, and/or standard deviation across subjects).*

Acquisition

Imaging type(s)	*Specify: functional, structural, diffusion, perfusion.*
Field strength	*Specify in Tesla*
Sequence & imaging parameters	*Specify the pulse sequence type (gradient echo, spin echo, etc.), imaging type (EPI, spiral, etc.), field of view, matrix size, slice thickness, orientation and TE/TR/flip angle.*
Area of acquisition	*State whether a whole brain scan was used OR define the area of acquisition, describing how the region was determined.*

Diffusion MRI ☐ Used ☐ Not used

Preprocessing

Preprocessing software — *Provide detail on software version and revision number and on specific parameters (model/functions, brain extraction, segmentation, smoothing kernel size, etc.).*

Normalization — *If data were normalized/standardized, describe the approach(es): specify linear or non-linear and define image types used for transformation OR indicate that data were not normalized and explain rationale for lack of normalization.*

Normalization template — *Describe the template used for normalization/transformation, specifying subject space or group standardized space (e.g. original Talairach, MNI305, ICBM152) OR indicate that the data were not normalized.*

Noise and artifact removal — *Describe your procedure(s) for artifact and structured noise removal, specifying motion parameters, tissue signals and physiological signals (heart rate, respiration).*

Volume censoring — *Define your software and/or method and criteria for volume censoring, and state the extent of such censoring.*

Statistical modeling & inference

Model type and settings — *Specify type (mass univariate, multivariate, RSA, predictive, etc.) and describe essential details of the model at the first and second levels (e.g. fixed, random or mixed effects; drift or auto-correlation).*

Effect(s) tested — *Define precise effect in terms of the task or stimulus conditions instead of psychological concepts and indicate whether ANOVA or factorial designs were used.*

Specify type of analysis: ☐ Whole brain ☐ ROI-based ☐ Both

Statistic type for inference (See Eklund et al. 2016) — *Specify voxel-wise or cluster-wise and report all relevant parameters for cluster-wise methods.*

Correction — *Describe the type of correction and how it is obtained for multiple comparisons (e.g. FWE, FDR, permutation or Monte Carlo).*

Models & analysis

n/a	Involved in the study
☐	☐ Functional and/or effective connectivity
☐	☐ Graph analysis
☐	☐ Multivariate modeling or predictive analysis

Functional and/or effective connectivity — *Report the measures of dependence used and the model details (e.g. Pearson correlation, partial correlation, mutual information).*

Graph analysis — *Report the dependent variable and connectivity measure, specifying weighted graph or binarized graph, subject- or group-level, and the global and/or node summaries used (e.g. clustering coefficient, efficiency, etc.).*

Multivariate modeling and predictive analysis — *Specify independent variables, features extraction and dimension reduction, model, training and evaluation metrics.*